

# Journal of Materials Chemistry A

Accepted Manuscript



This is an *Accepted Manuscript*, which has been through the Royal Society of Chemistry peer review process and has been accepted for publication.

*Accepted Manuscripts* are published online shortly after acceptance, before technical editing, formatting and proof reading. Using this free service, authors can make their results available to the community, in citable form, before we publish the edited article. We will replace this *Accepted Manuscript* with the edited and formatted *Advance Article* as soon as it is available.

You can find more information about *Accepted Manuscripts* in the [Information for Authors](#).

Please note that technical editing may introduce minor changes to the text and/or graphics, which may alter content. The journal's standard [Terms & Conditions](#) and the [Ethical guidelines](#) still apply. In no event shall the Royal Society of Chemistry be held responsible for any errors or omissions in this *Accepted Manuscript* or any consequences arising from the use of any information it contains.



## Large Active Layer Thickness Toleration of High-efficiency Small-molecule Solar Cells

Qian Zhang,<sup>a</sup> Bin Kan,<sup>a</sup> Xiangjian Wan,<sup>\*a</sup> Hua Zhang,<sup>b</sup> Feng Liu,<sup>c</sup> Miaomiao Li,<sup>a</sup> Xuan Yang,<sup>a</sup> Yunchuang Wang,<sup>a</sup> Wang Ni,<sup>a</sup> Thomas P Russell,<sup>d</sup> Yan Shen<sup>\*b</sup> and Yongsheng Chen<sup>\*a</sup>

Received 00th January 20xx,  
Accepted 00th January 20xx

DOI: 10.1039/x0xx00000x

www.rsc.org/

High-efficiency organic solar cells with large active layer thickness toleration is highly demanded to meet the challenges in feasible commercial production on a large scale. Generally, devices with thick active layer are preferred because it allows both the formation of more uniform film and the effective utilization of incident light. In this work, solar cell devices with layer thicknesses ranging from 65 to 370 nm based on a small molecule donor DR3TSBDT and electron acceptor PC<sub>71</sub>BM were fabricated and the thickness dependence of photovoltaic performance was systematically studied. High power conversion efficiencies (PCEs) were well-maintained in a wide layer thickness range, and for devices with layer thickness at 280 and 370 nm, off only ~8% and 20% from its best PCE of 9.95% at 120 nm were achieved, respectively. With systematic investigations, the well-maintained high performance are attributed to the facts that both the nearly ideal morphology (bi-continuous interpenetrating crystalline nano-fibrillar structure) of the active layer and hole mobility remained hardly changed in the wide thickness range. Also as expected, with increasing thickness, larger transport resistance, charge recombination and transit time were observed, which made the fill factor lower. But these inferior factors were largely compensated by the increased current, and thus well-maintained high performance was achieved.

With the rapid development in the last few years, while the power conversion efficiencies (PCEs) of organic solar cells (OSCs) have increased to over 10%,<sup>1-14</sup> one of the remaining challenges for high-throughput production is to develop materials and devices which can tolerate large active layer thickness variations. As accurate thickness control, if not impossible at industry scale, would dramatically increase the capital investment and thus processing cost. Thick active layers are preferred because it is easy to form uniform films with lower defect density (pinholes) and enhance the reproducibility of OSCs.<sup>15,16</sup> In addition, increasing active layer thickness can also realize more effective utilization of incident light. However, the majority of reported devices so far based on both polymers and small molecules with high PCEs were typically with thin active layers of ~100 nm, and most of the device performances were also sensitive to the active layer thickness.<sup>1,4-6,17-20</sup> Generally, active layer thickness over 200 nm is a prerequisite in the views of the feasibility and cost

issue in the future large scale printing process.<sup>16,21</sup>

To the best of our knowledge, only a few reports studied the active layer thickness dependence of the photovoltaic performance, especially with thickness above 300 nm.<sup>22-32</sup> In addition, there is no report about the issue based on the solution processed small molecules based devices. In this work, using one of the best reported small molecule donors, DR3TSBDT,<sup>33</sup> devices with a series of active layer thickness in the range of 65-370 nm were fabricated and the thickness dependence of photovoltaic performance was systematically studied. High power conversion efficiencies (PCEs) were maintained in a wide range of active layer thickness. PCEs of 9.15% and 7.93% were achieved with active layer thickness at 280 and 370 nm, off only ~8% and 20% from the best PCE of 9.95% at the active layer thickness of 120 nm, respectively. Systematic morphological characterization studies indicate that all active layers with various thicknesses possessed similar morphology with optimal highly ordered nano-fibrillar structures, which is beneficial for the efficient exciton dissociation and charge transport. Furthermore, there were nearly no change in the device hole mobility when the active layer thickness increased. And with increasing active layer thickness, the transport resistance, charge recombination and transit time increased, which made the fill factor (FF) become lower. But the reduction of FF was largely offset by the increased current resulting from the increased overall light absorption, and thus well-retained high performance for thick devices was observed.

<sup>a</sup> State Key Laboratory and Institute of Elemento-Organic Chemistry and Centre for Nanoscale Science and Technology, Institute of Polymer Chemistry and Collaborative Innovation Center of Chemical Science and Engineering (Tianjin), College of Chemistry, Nankai University, Tianjin 300071, China.

<sup>b</sup> Wuhan National Laboratory for Optoelectronics, School of Optical and Electronic Information, Huazhong University of Science and Technology, Wuhan, Hubei 430074, China.

<sup>c</sup> Materials Science Divisions, Lawrence Berkeley National Lab, Berkeley 94720, United States.

<sup>d</sup> Department of Polymer Science and Engineering, University of Massachusetts, Amherst 01003, United States.

Electronic Supplementary Information (ESI) available: [materials, characterizations, instruments, Figure S1-S8 and Table S1-S4]. See DOI: 10.1039/x0xx00000x

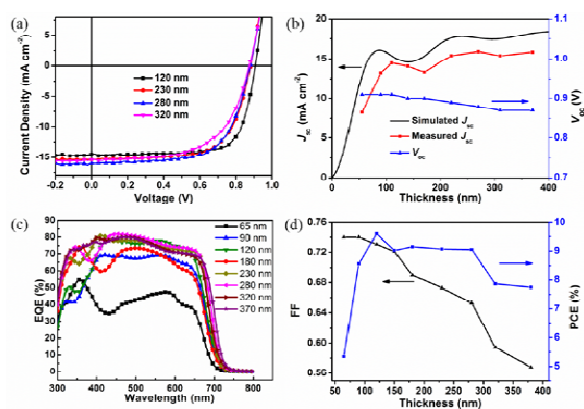


Fig. 1. a) Current density versus voltage ( $J$ - $V$ ) characteristics for DR3TSBDT:PC<sub>71</sub>BM devices with 120, 230, 280 and 320-nm thick active layer. b) Variation of simulated (black line) and measured  $J_{sc}$  (red line) and  $V_{oc}$  (blue line) with active layer thickness in the range of 65–370 nm. c) Corresponding EQE spectra for the devices. d) Average FF and PCE versus active layer thickness for the devices.

Devices based on the blend system of DR3TSBDT and [6,6]-phenyl-C<sub>71</sub> butyric acid methyl ester (PC<sub>71</sub>BM) with different active layer thickness were fabricated with the similar procedures we have reported.<sup>33</sup> The concentrations of the mixture of DR3TSBDT and PC<sub>71</sub>BM and spin-coating speeds were varied to form different thickness of the active layer. The average solar cell parameters with active layer thickness varying 65–370 nm were summarized in Table 1. The typical current density-voltage ( $J$ - $V$ ) characteristic curves for devices with active layer thickness of 120, 230, 280 and 320 nm were shown in Fig. 1a. As shown in Table 1 and Fig. 1b, the  $V_{oc}$  of the devices with different active layer thickness nearly remained unchanged with values from 0.87 to 0.91 V. While, the  $J_{sc}$  of the devices initially increased with increasing active layer thickness resulting from the increased absorption, then decreased due to the optical interference, and then remained nearly constant with further increasing the active layer thickness. This is consistent with the optical simulation results calculated by transfer-matrix methods (TMM) as demonstrated in Fig. 1b, which reveals that the first interference minima is at thickness of 180 nm and the optical absorption becomes nearly impervious to destructive interference when the active layer thickness is > 200 nm. Fig. 1c shows the external quantum efficiency (EQE) spectra for the devices with different active layer thickness. The device with 65 nm thick active layer exhibited a low EQE of 47% at 580 nm. And high EQE of 69% at 580 nm was achieved when the active layer thickness increased to 90 nm. With further increasing the thickness in the range of 120 to 370 nm, the devices almost displayed a relatively flat EQE over 70% between 350 and 700 nm. The integrated current density from the EQE spectra is consistent with the measured  $J_{sc}$  within 5% deviation. From Fig. 1d, the FF decreased with the increase of active layer thickness. The decreased FF for thick active layer was attributed to the

Table 1. The average photovoltaic parameters for DR3TSBDT:PC<sub>71</sub>BM devices with active layer thickness varying 65–370 nm under AM 1.5 G solar illumination. The best PCEs are provided in parentheses.

Thickness (nm)	$V_{oc}$ (V)	$J_{sc}$ (mA cm <sup>-2</sup> )	$J_{sc,EQE}$ (mA cm <sup>-2</sup> )	FF (%)	PCE (%)
65	0.91±0.1	8.23±0.20	7.86	74.0±0.2	5.34(5.55)
90	0.91±0.1	13.17±0.22	12.57	74.0±0.1	8.56(8.88)
120	0.91±0.1	14.45±0.18	14.10	73.1±0.3	9.60(9.95)
150	0.90±0.1	14.00±0.23	13.35	72.1±0.3	9.02(9.13)
180	0.90±0.1	13.20±0.15	12.73	69.0±0.2	8.15(8.26)
230	0.89±0.1	15.22±0.25	14.69	67.3±0.2	9.07(9.20)
280	0.88±0.1	15.82±0.15	15.23	65.3±0.3	9.05(9.15)
320	0.87±0.1	15.21±0.23	14.68	59.4±0.5	7.86(8.15)
370	0.87±0.1	15.66±0.20	15.11	56.8±0.3	7.74(7.97)

improved transport resistance, charge accumulation and transit time with increasing active layer thickness, which would be discussed below. However, the reduction of FF was largely compensated by the increased  $J_{sc}$  and thus high performances were well-maintained for thick active layer devices. From Fig. 1d, high PCEs of 9.15% and 7.97% were retained with the active layer thickness even at 280 and 370 nm, respectively. Note this is within 8% and 20% off from the best performance for the device with active layer thickness at 120 nm, respectively.

The thickness dependence of FF is closely associated with the electrical property variations in the devices, which were systematically investigated by impedance spectroscopy (IS)<sup>34,35</sup> under 20 mW/cm<sup>2</sup> illumination intensity using a white light emitting diode. Representative impedance data, in the form of Nyquist curves for devices with different active layer thickness measured at different bias close to the  $V_{oc}$  were shown in Fig. S3. IS data were modelled using equivalent circuit (shown in the inset Fig. S3a) to identify physical parameters: a series resistance  $R_s$ , a transport resistance  $R_1$ , a constant phase element (CPE<sub>1</sub>) associated with the depletion region within the active layer, and a recombination resistance  $R_{rec}$  in parallel with a CPE<sub>2</sub>.<sup>36</sup> CPE represents a non-ideal capacitor which includes an adjustable parameter to compensate for non-homogeneity of the blocking interface (surface states, etc.) when put in parallel with a resistor. The capacitance for CPE is

$$C_{\mu} = (Y_0 R)^{\frac{1}{n}} / R$$

calculated by using the equation  $C_{\mu} = (Y_0 R)^{\frac{1}{n}} / R$ , where  $Y_0$  and  $n$  are the two parameters of CPE obtained from equivalent circuit fitting. The  $R_s$  represents resistive losses in the ITO and PEDOT:PSS. The  $R_1$ /CPE<sub>1</sub> combination contributes to the high frequency response in the Nyquist plot, which is related to the information of electronic transport in bulk as well as dielectric contributions. The  $R_{rec}$ /CPE<sub>2</sub> arc contributes to the low frequency response, which is associated with the charge carrier recombination

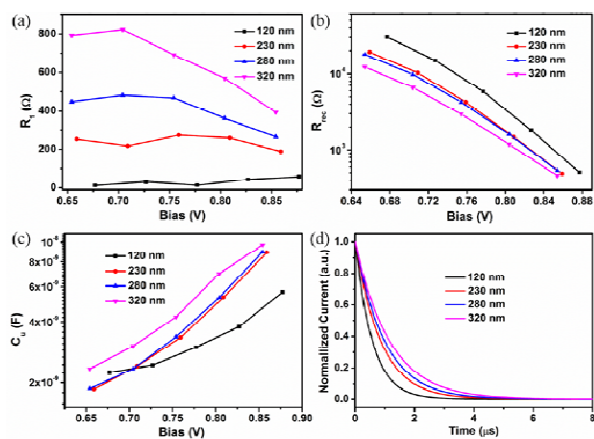


Fig. 2. a) The transport resistance  $R_1$ , b) Recombination resistance  $R_{rec}$  and c) Chemical capacitance  $C_\mu$  as a function of different bias close to the open circuit voltage obtained from electrochemical impedance spectroscopy. d) Comparison of normalized short-circuit current dynamics of DR3TSBDT:PC<sub>71</sub>BM cells with 120, 230, 280 and 320 nm-thick active layers.

process in the active layer. The fitting parameters were demonstrated in Electronic Supplementary Information. First, the transport resistance  $R_1$  improved with the increase of layer thickness as shown in Fig. 2a. Second, from Fig. 2b, with increasing layer thickness, the capacitance  $C_\mu$  obtained from the low frequency regime increased, indicative of more carrier accumulation inside active layer.<sup>37</sup> Physically, the accumulated photo-generated carriers that increase  $C_\mu$  have two ways to escape: collected through the external pathway or recombined through the recombination resistor ( $R_{rec}$ ). So decreased  $R_{rec}$  represents more probability to carrier recombination with increasing layer thickness (Fig. 2c). The recombination lifetime, which is a product of  $C_\mu$  and  $R_{rec}$ . Fig. S4b presented the electron lifetime as the function of the charge density for devices with different active layer thickness. At a given charge density, the device with 120 nm-thick film showed the longest electron lifetime. A shorter electron lifetime was observed for the device with thicker active layer (Fig. S4b), indicating the accumulated charge in the active layer plays important role on the interfacial charge recombination process. This result agrees well with the observation on  $V_{oc}$  and FF for various devices, which decrease as the active layer thickness increase.

The dynamics dependent on active layer thickness for DR3TSBDT:PC<sub>71</sub>BM devices were also studied using transient photocurrent (TPC)<sup>38</sup> measurements at the short circuit condition under 1 ms step pulse illumination. Fig. 2d presented the normalized photocurrent transients with increasing active layer thickness. The transit time was shown in Table S5. It clearly shows that photocurrent dynamics systematically becomes slower with increasing thickness, suggesting longer extraction time and the increase in the distance carriers need to traverse.<sup>39</sup>

In order to further understand the reduction of FF with

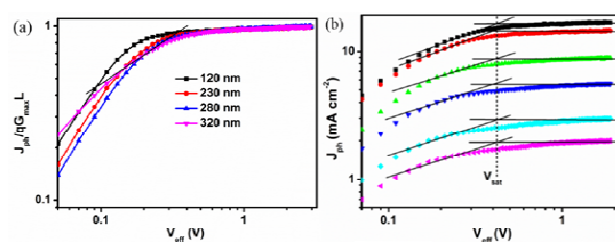


Fig. 3. a) Effective photocurrent density ( $J_{ph}$ ) normalized by  $J_{sat}$  as a function of effective voltage ( $V_{eff}$ ) under 100 mW cm<sup>-2</sup> illumination for DR3TSBDT:PC<sub>71</sub>BM cells with 120, 230, 280 and 320 nm-thick active layer (The solid black line indicates square root). b)  $J_{ph}$  of a 320 nm-thick DR3TSBDT:PC<sub>71</sub>BM cell versus  $V_{eff}$  at different intensities (10 to 100 mW cm<sup>-2</sup>). Solid lines indicate square root and saturation regimes as a guide for the eye where  $V_{sat}$  indicates the saturation voltage.

increasing active layer thickness, the relationship of photocurrent density ( $J_{ph}$ ) versus effective voltage ( $V_{eff}$ ) or light intensity ( $P_{in}$ ) for the devices with different active layer thickness were studied. The normalized photocurrent-effective voltage ( $J_{ph}-V_{eff}$ ) curves for DR3TSBDT:PC<sub>71</sub>BM devices with 120, 230, 280 and 320 nm-thick active layers are shown in Fig. 3a. The photocurrent is defined as  $J_{ph} = J_L - J_D$ , where  $J_L$  and  $J_D$  are the current density under illumination and in the dark, respectively. For  $V_{eff} = V_o - V_a$ ,  $V_o$  is the voltage at which  $J_{ph} = 0$  and  $V_a$  is the applied voltage. The curves for all three devices with 120, 230 and 280 nm look very similar despite the increase in the active layer thickness. When  $V_{eff} > 0.20$  V, the photocurrent of the three devices saturated with increasing voltage. In this saturation regime, the internal field was strong enough to separate excitons and efficiently extract photo-generated carriers. The voltage corresponding to the short circuit conditions (about 0.89 V) fell in the saturation regime ( $J_{sat}$ ), indicative of efficient exciton dissociation and charge collection. These results correlate well with the high FFs of 65% to 73% obtained for the above three devices. However, when the active layer thickness increased to 320 nm, a square-root effective voltage dependence on  $J_{ph}$  was observed (as shown by the solid line in Fig. 3a). The origin of such a square root dependence of the photocurrent has been explained by Goodman and Rose in 1971, which is an indication of either recombination-limited (Equation 1) or space-charge-limited (SCL) photocurrent (Equation 2) below:<sup>40</sup>

$$J_{ph} = qG\sqrt{\mu_{h(e)}\tau_{h(e)}}\sqrt{V} \quad (1)$$

$$J_{ph} \leq (qG)^{0.75} \left(\frac{9}{8} \epsilon_0 \epsilon_r \epsilon_h\right)^{0.25} \sqrt{V} \quad (2)$$

Where  $G$  is the generation rate of free charge carriers.

For the former case, a low mobility or short lifetime of the free carriers, due to recombination or trapping, lead to the mean electron or hole (or both) drift length becoming smaller than the active layer thickness and thus recombination of charge carriers becomes considerable.<sup>40,41</sup> For the latter case, at high

light intensities the build-up of space charges (which is the origin of the non-uniform electric field) reaches a fundamental limit.<sup>42</sup> Analysing the light intensity dependent of the photocurrent and the point at which the square root regime forms a transition into the saturation regime  $V_{\text{sat}}$  is an effective method to distinguish between these two physically distinct cases. While in the first (recombination-limited) case the photocurrent scales linearly with light intensity, SCL photocurrent scales with a three-fourth power law dependence. Besides,  $V_{\text{sat}}$  is either independent on light intensity (recombination-limited) or scales with a one half power on light intensity (SCL case).<sup>40</sup>

Photocurrent of a 320 nm-thick DR3TSBDT:PC<sub>71</sub>BM solar cell versus  $V_{\text{eff}}$  at different intensities was shown in Fig. 3b. Neutral density filters were used to control the incident light intensity, which was varied from 10 to 100 mW cm<sup>-2</sup>. It is clear that  $V_{\text{sat}}$  does not change with decreasing light intensity, as expected for a recombination-limited photocurrent. Furthermore, for the solar cell with a 320 nm-thick active layer,  $J_{\text{ph}}$  showed a sub-linear dependence on light intensity with the

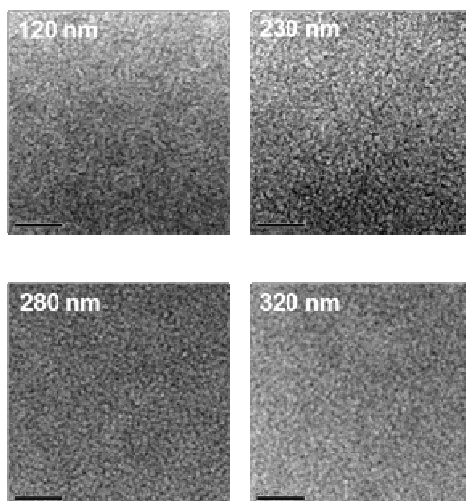


Fig. 4. TEM images of DR3TSBDT:PC<sub>71</sub>BM with different active layer thickness. The scale bar is 200 nm.

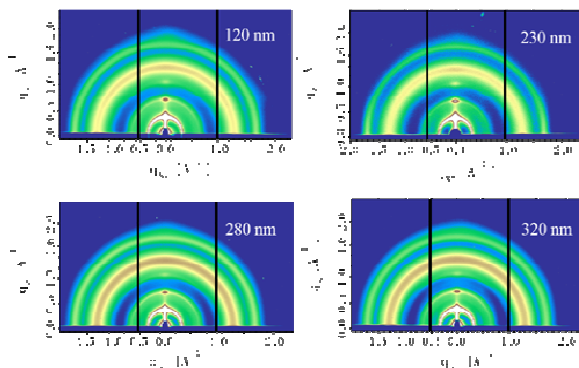


Fig. 5. The GIXD diffraction profiles of DR3TSBDT:PC<sub>71</sub>BM films with different thickness.

slope of the linear fit to 0.902 at the maximum power-output point (Fig. S5), which could also be a sign of significant bimolecular recombination.<sup>41</sup> Therefore, the photocurrent observed for DR3TSBDT:PC<sub>71</sub>BM devices clearly showed the fingerprints of a recombination-limited photocurrent.<sup>40</sup> This may be due to the relatively low mobility of  $6.13 \times 10^{-4} \text{ cm}^2 \text{ V}^{-1} \text{ s}^{-1}$  compared with reported polymers.<sup>22,29</sup> So higher rate of forming photo-generated charge carriers in thick devices resulted in more charge accumulation and bimolecular recombination, which was consistent with its relatively larger transport resistance and chemical capacitance discussed above. Thus, the photovoltaic performance for 320 nm-thick devices was sharply reduced.

The morphology of the active layers can be a determining factor for the well-maintained high photovoltaic performance. The nanoscale morphology of DR3TSBDT:PC<sub>71</sub>BM blends with different thickness were measured by atomic force microscopy (AFM) and high-resolution transmission electron microscopy (HR-TEM). From AFM images (Fig. S6), all films with different thickness exhibited a bi-continuous interpenetrating network and small root-mean-square (RMS) roughness of about 1 nm, which indicated these films were smooth and uniform. From TEM images (Fig. 4), no particular different morphology such as large size aggregation of nanoparticles was found for thick active layers. And well-distributed nano-fibrillar structures where a bi-continuous interpenetrating network could be observed, which are favourable for the exciton dissociation and charge transport, and thus high  $J_{\text{sc}}$  and FF.

To further understand the microstructures of the active layers with different thickness, grazing incidence X-ray diffraction (GIXD) were measured (Fig. 5). The line-cuts of all diffractions are shown in Fig. S7. All films show multiple higher order (h00) reflections, indicative of a long-range order and lateral packing of the backbones. In addition, the strong reflection of (010) peaks characteristic of the  $\pi$ - $\pi$  stacking distance (3.61 Å), show a large azimuthally distribution for all films, which suggests the mixture of face-on and edge-on packing. Similar patterns behaviour in the GIXDs indicates that DR3TSBDT possesses the same ordered structure in the blend composition for a wide range of thicknesses. Thus, all films with various thicknesses exhibited similar morphology with highly ordered nano-fibrillar structures, which is beneficial for efficient exciton diffusion and dissociation and charge transport. Besides, hole mobility for different thickness-devices were measured using space-charged-limited-current (SCLC) method. Notably, the magnitude of the hole mobility of DR3TSBDT remained the same for all active layer thickness from 120 nm to 370 nm and showed negligible changes with a value of  $3.20 \times 10^{-4} \text{ cm}^2 \text{ V}^{-1} \text{ s}^{-1}$  at 370 nm-thick film (Fig. S8). These morphology and SCLC results are consistent with the maintained high performance of thick devices.

## Conclusion

To conclude, devices with a series of active layer thickness in the range of 65–370 nm based on the small molecule donor, DR3TSBDT, were fabricated and the thickness dependence of photovoltaic performance, mechanisms and morphology were systematically investigated. All active layers with various thicknesses possessed similar morphology with highly ordered nano-fibrillar structures, which are beneficial for efficient exciton dissociation and charge transport. And the hole mobility hardly changed with increasing active layer thickness. Thick active layer enabled more light absorption, yielding a high  $J_{sc}$  of  $\sim 15.92 \text{ mA cm}^{-2}$ . Nevertheless, with the increase of active layer thickness, the transport resistance, charge accumulation and the distance carriers needed to traverse increased, thus leading to more bimolecular recombination and decreased FF. However, the inferior factor of FF reduction was largely compensated by the increased absorption, and thus high PCEs of 9.15% was achieved with the active layer thickness at 280 nm. And devices with active layer thickness at 370 nm retained 80% of its best PCE at 120 nm. The high efficiency for thick active layers and its high toleration of active layer thickness variations make DR3TSBDT:PC<sub>71</sub>BM films a promising candidate for low-cost, high-throughput industry photovoltaic applications.

## Acknowledgements

The authors gratefully acknowledge the financial support from MoST (2014CB643502), NSFC (51373078, 51422304, 91433101), PCSIRT (IRT1257) and Tianjin city (13RCGFGX01121).

## Notes and references

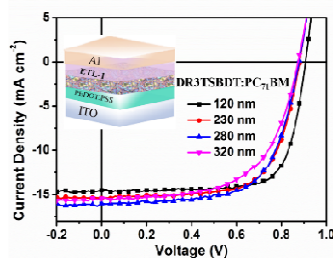
- Z. He, B. Xiao, F. Liu, H. Wu, Y. Yang, S. Xiao, C. Wang, T. P. Russell and Y. Cao, *Nat. Photonics* 2015, **9**, 174.
- Y. Liu, J. Zhao, Z. Li, C. Mu, W. Ma, H. Hu, K. Jiang, H. Lin, H. Ade and H. Yan, *Nat. Commun.* 2014, **5**, 5293.
- B. Kan, M. Li, Q. Zhang, F. Liu, X. Wan, Y. Wang, W. Ni, G. Long, X. Yang, H. Feng, Y. Zuo, M. Zhang, F. Huang, Y. Cao, T. P. Russell and Y. Chen, *J. Am. Chem. Soc.* 2015, **137**, 3886.
- C. Liu, C. Yi, K. Wang, Y. Yang, R. S. Bhatta, M. Tsige, S. Xiao and X. Gong, *ACS Appl. Mater. Interfaces* 2015, **7**, 4928.
- L. Ye, S. Zhang, W. Zhao, H. Yao and J. Hou, *Chem. Mater.* 2014, **26**, 3603.
- L. K. Jagadamma, M. Al-Senani, A. El-Labban, I. Gereige, G. O. Ngongang Ndjawa, J. C. D. Faria, T. Kim, K. Zhao, F. Cruciani, D. H. Anjum, M. A. McLachlan, P. M. Beaujuge and A. Amassian, *Adv. Energy Mater.* 2015, **5**, 1500204.
- L. Zuo, C. Chang, C. Chueh, S. Zhang, H. Li, A. K. Y. Jen and H. Chen, *Energy Environ. Sci.* 2015, **8**, 1712.
- L. Huo, T. Liu, X. Sun, Y. Cai, A. J. Heeger and Y. Sun, *Adv. Mater.* 2015, **27**, 2938.
- S. Zhang, L. Ye, W. Zhao, B. Yang, Q. Wang and J. Hou, *Sci. China Chem.* 2015, **58**, 248.
- J. Chen, C. Cui, Y. Le, L. Zhou, Q. Ou, C. Li, Y. Li and J. Tang, *Adv. Mater.* 2015, **27**, 1035.
- L. Nian, W. Zhang, N. Zhu, L. Liu, Z. Xie, H. Wu, F. Wurthner and Y. Ma, *J. Am. Chem. Soc.* 2015, **137**, 6995.
- Y. Liu, C. Chen, Z. Hong, J. Gao, Y. Yang, H. Zhou, L. Dou, G. Li and Y. Yang, *Sci. Rep.* 2013, **3**, 3356.
- H. Zhou, Y. Zhang, C. Mai, S. D. Collins, G. C. Bazan, T. Q. Nguyen and A. J. Heeger, *Adv. Mater.* 2015, **27**, 1767.
- A. R. M. Yusoff, D. Kim, H. P. Kim, F. K. Shneider, W. J. Silva and J. Jang, *Energy Environ. Sci.*, 2015, **8**, 303.
- P. W. M. Blom, V. D. Mihailetschi, L. J. A. Koster and D. E. Markov, *Adv. Mater.* 2007, **19**, 1551.
- T. D. Nielsen, C. Cruickshank, S. Foged, J. Thorsen and F. C. Krebs, *Sol. Energy Mater. Sol. Cells* 2010, **94**, 1553.
- Z. He, C. Zhong, S. Su, M. Xu, H. Wu and Y. Cao, *Nat. Photonics* 2012, **6**, 591.
- Q. Zhang, B. Kan, F. Liu, G. Long, X. Wan, X. Chen, Y. Zuo, W. Ni, H. Zhang, M. Li, Z. Hu, F. Huang, Y. Cao, Z. Liang, M. Zhang, T. P. Russell and Y. Chen, *Nat. Photonics* 2015, **9**, 35.
- L. Lu, W. Chen, T. Xu and L. Yu, *Nat. Commun.* 2015, **6**, 7327.
- C. Li, C. Chang, Y. Zang, H.-X. Ju, C.-C. Chueh, P.-W. Liang, N. Cho, D. S. Ginger and A. K. Y. Jen, *Adv. Mater.* 2014, **26**, 6262.
- F. C. Krebs, *Sol. Energy Mater. Sol. Cells* 2009, **93**, 1636.
- W. Li, K. H. Hendriks, W. S. C. Roelofs, Y. Kim, M. M. Wienk and R. A. J. Janssen, *Adv. Mater.* 2013, **25**, 3182.
- S. C. Price, A. C. Stuart, L. Yang, H. Zhou and W. You, *J. Am. Chem. Soc.* 2011, **133**, 4625.
- Y. Zhang, J. Liu, L. Zhang, J. Fang, W. Zhang and Z. Liu, *Chinese J. Org. Chem.* 2014, **34**, 1021.
- C. E. Small, S. W. Tsang, S. Chen, S. Baek, C. M. Amb, J. Subbiah, J. R. Reynolds and F. So, *Adv. Energy Mater.* 2013, **3**, 909.
- Z. Lu, B. Jiang, X. Zhang, A. Tang, L. Chen, C. Zhan and J. Yao, *Chem. Mater.* 2014, **26**, 2907.
- R. Kroon, A. Diaz de Zerio Mendaza, S. Himmelberger, J. Bergqvist, O. Bäcke, G. C. Faria, F. Gao, A. Obaid, W. Zhuang, D. Gedefaw, E. Olsson, O. Inganäs, A. Salleo, C. Müller and M. R. Andersson, *J. Am. Chem. Soc.* 2014, **136**, 11578.
- S. Lee, S. Nam, H. Kim and Y. Kim, *Appl. Phys. Lett.* 2010, **97**, 103503.
- T. L. Nguyen, H. Choi, S. J. Ko, M. A. Uddin, B. Walker, S. Yum, J. E. Jeong, M. H. Yun, T. J. Shin, S. Hwang, J. Y. Kim and H. Y. Woo, *Energy Environ. Sci.* 2014, **7**, 3040.
- K. Sun, Z. Xiao, S. Lu, W. Zajaczkowski, W. Pisula, E. Hanssen, J. M. White, R. M. Williamson, J. Subbiah, J. Ouyang, A. B. Holmes, W. W. H. Wong and D. J. Jones, *Nat. Commun.* 2015, **6**, 6013.
- H. Choi, S.-J. Ko, T. Kim, P.-O. Morin, B. Walker, B. H. Lee, M. Leclerc, J. Y. Kim and A. J. Heeger, *Adv. Mater.* 2015, **27**, 3318.
- V. Vohra, K. Kawashima, T. Kakara, T. Koganezawa, I. Osaka, K. Takimiya and H. Murata, *Nat. Photonics* 2015, **9**, 403.
- B. Kan, Q. Zhang, M. Li, X. Wan, W. Ni, G. Long, Y. Wang, X. Yang, H. Feng and Y. Chen, *J. Am. Chem. Soc.* 2014, **136**, 15529.
- G. Garcia-Belmonte, P. P. Boix, J. Bisquert, M. Sessolo and H. J. Bolink, *Sol. Energy Mater. Sol. Cells* 2010, **94**, 366.
- G. Garcia-Belmonte, A. Munar, E. M. Barea, J. Bisquert, I. Ugarte and R. Pacios, *Org. Electron.* 2008, **9**, 847.
- G.-H. Kim, H.-K. Song and J. Y. Kim, *Sol. Energy Mater. Sol. Cells* 2011, **95**, 1119.
- G. Perrier, R. de Bettignies, S. Berson, N. Lemaitre and S. Guillerez, *Sol. Energy Mater. Sol. Cells* 2012, **101**, 210.
- C. G. Shuttle, A. Maurano, R. Hamilton, B. O'Regan, J. C. de Mello and J. R. Durrant, *Appl. Phys. Lett.* 2008, **93**, 183501.
- Z. Li, F. Gao, N. C. Greenham and C. R. McNeill, *Adv. Funct. Mater.* 2011, **21**, 1419.
- M. Lenas, M. Morana, C. J. Brabec and P. W. M. Blom, *Adv. Funct. Mater.* 2009, **19**, 1106.

## ARTICLE

Journal Name

- 41 K. R. Choudhury, J. Subbiah, S. Chen, P. M. Beaujuge, C. M. Amb and J. R. Reynolds, *F. So, Sol. Energy Mater. Sol. Cells* 2011, **95**, 2502.
- 42 V. D. Mihailetschi, J. Wildeman, P. W. M. Blom, *Phys. Rev. Lett.* 2005, **94**, 126602.
- 43 C. M. Proctor, C. Kim, D. Neher and T.-Q. Nguyen, *Adv. Funct. Mater.* 2013, **23**, 3584.

## Table of Contents



The thickness dependence of photovoltaic performance for the small-molecule DR3TSBDT:PC<sub>71</sub>BM based devices was systematically investigated and the power conversion efficiencies are relatively insensitive to the thickness.